



Synthesis and characterization of V-doped TiO₂ nanoparticles through polyol method with enhanced photocatalytic activities

Khaled Belfaa¹ · Mohamed Saber Lassoued¹ · Salah Ammar¹ · Abdellatif Gadri¹

Received: 26 January 2018 / Accepted: 10 April 2018 / Published online: 13 April 2018
© Springer Science+Business Media, LLC, part of Springer Nature 2018

Abstract

This work reports the synthesis of vanadium-doped titanium dioxide nanoparticles using titanium chloride and ethylene glycol as precursor and solvent respectively. The properties of as-prepared samples were investigated by X-ray diffractometry, scanning electron microscopy, Fourier transform infrared (FTIR) spectroscopy, diffuse reflectance, and thermal analysis. X-ray diffraction patterns indicate that the TiO₂ nanoparticles obtained after calcination at 500 °C under air atmosphere has the anatase phase with a tetragonal structure and the crystallite sizes were in the range 16.83–12.27 nm. The transmission electron microscopy was used to detect the morphology of synthesized nanoparticles. The functional groups present in the samples were identified by FTIR study. From the optical studies, there is a blue shift in the absorption edge for our samples that can be attributed to the presence of V in the TiO₂. For V doped TiO₂ nanoparticles the optical band gap varies between 3.18 and 2.60 eV with the increase of V concentration. The TGA findings allow the thermal cycle determination of samples whereas DTA findings allow the phase transition temperature identification. Finally, the evaluation of the photocatalytic activity is carried out using methyl blue as model of chemical pollutants in UV irradiation conditions and followed satisfactory the pseudo first order according to the Langmuir–Hinshelwood model.

1 Introduction

Titanium dioxide (TiO₂) has attracted significant attention from researchers because of the lot interesting physical and chemical properties. It has high corrosion resistance and chemical stability, biological inertness, non-toxic as well as its low cost. These properties make it suitable for a variety of applications, traditionally such as pigments, cosmetic then more recently according to photo generation of electron hole as photocatalysts, as particles for solar cells and as coating with self-cleaning properties [1–6]. From point of view of structural properties, Titanium dioxide has three types of crystal forms, which are brookite, anatase and rutile. By increasing the temperature, the amorphous phase convert to the anatase phase then transformed irreversibly to rutile phase. It has been previously reported that anatase to rutile transformation in synthetic TiO₂ usually occurs

at a temperature of 600–700 °C. Brookite crystallizes in orthorhombic structure [7]. It is unstable phase, so it has no industrial value, while the colloidal phase preparation methods for TiO₂ favor generally the tetragonal structure with an anatase form and lattice constants equal to $a = 3.785$ (Å) and $c = 9.513$ (Å) [8, 9] and it is favor for photocatalytic application (IDD 41-1445).

Several methods of synthesis methods (polyol, precipitation, micellar route, sol–gel, thermal decomposition of organometallic precursors, etc.) have been developed to produce these materials as nanoparticles [10–20]. In this work, we investigate the polyol method to synthesize nanoparticle of V-doped TiO₂ with enhanced photocatalytic activities because it offers many advantages such its simple preparation, high purity, good reproducibility, low operation temperature, high crystalline quality, even with any additional heat treatment in some case when it used others type treatment like microondes [21].

Recently, conventional polyol process through utilization of metal precursor and ethylene glycol has been developed as a powerful alternative to preparation of TiO₂ with metal or nonmetal doping. Doping oxide titanium is one of the promising approaches which extend the photo response of TiO₂ from the ultraviolet into the visible region [22]. Mansour

✉ Khaled Belfaa
belfaakhaled@yahoo.com

¹ Unité de Recherche Electrochimie, Matériaux et Environnement UREME (UR17ES45), Faculté des Sciences de Gabès, Université de Gabès, Cité Erriadh, 6072 Gabès, Tunisia

et al. [23] have reported the processing of the titanium oxide nanoparticles via co-precipitation synthesis technique using double distilled water as a solvent. However in this work, TiO_2 nanoparticles were synthesized by polyol method under various vanadium doped titanium dioxide nanoparticles concentration. The nanoparticles are well characterized for their structural, morphological and optical properties by various characterization techniques such as the X-ray diffraction, transmission electron microscopy (TEM), Fourier Transform Infra-Red (FT-IR), UV–visible analysis, TGA and DTA thermal analysis and photoluminescence (PL). Finally, the photocatalytic properties of the materials prepared were investigated in the case of the photodegradation of MB under UV-light illumination, the greatest activity being found for the 8% at V-doped TiO_2 nanomaterials.

2 Experimental

TiO_2 were synthesized by polyol method used the salts TiCl_4 as titanium source and ethylene glycol as solvent. It was prepared from (4.26 g) of precursor which was dissolved in 75 ml of ethylene glycol under stirring (S1). In other hand appropriate amount of $\text{CH}_3\text{COONa}\cdot 3\text{H}_2\text{O}$ (16.2 g) was dissolved in 75 ml (S2). After the disappearing of the turbidity, we added drop wise the S2 to S1. Then the mixture was heated for 3 h at 160 °C. The synthesis of V doped TiO_2 is the same as pure we dissolved appropriate amount of ammonium methavanadate corresponding to $[\text{V}]/[\text{Ti}]$ from 2 to at 8% in 50 ml of ethylene glycol and added to S1 (in this step the volumes of S1 and S2 were 50 ml). The resulting precipitates were separated by centrifugation, washed several time with ethanol and water and finally dried at 80 °C for 12 h. Annealing of the dried sample in air at 500 °C for 4 h led to obtain TiO_2 (white nanopowders) and V-doped TiO_2 (yellowish nanopowders) (Fig. 1).

2.1 Investigation techniques

The characterization of the prepared compound was performed using X-ray diffraction, Transmission electron microscope (TEM), Fourier Transform Infra-Red (FT-IR), UV–visible analysis (UV), thermal analyses (TGA and DTA) and photoluminescence (PL).

2.2 Characterization

The crystalline quality and the grain size of the samples were evaluated using X-ray diffraction (XRD) measurements. The study was carried out using an AXS Simens D5000 diffractometer equipped with a source delivering a monochromatic $\text{Cu K}\alpha$ 1 radiation ($\lambda = 1.54056 \text{ \AA}$). A continuous scan mode was employed to collect data from 20°

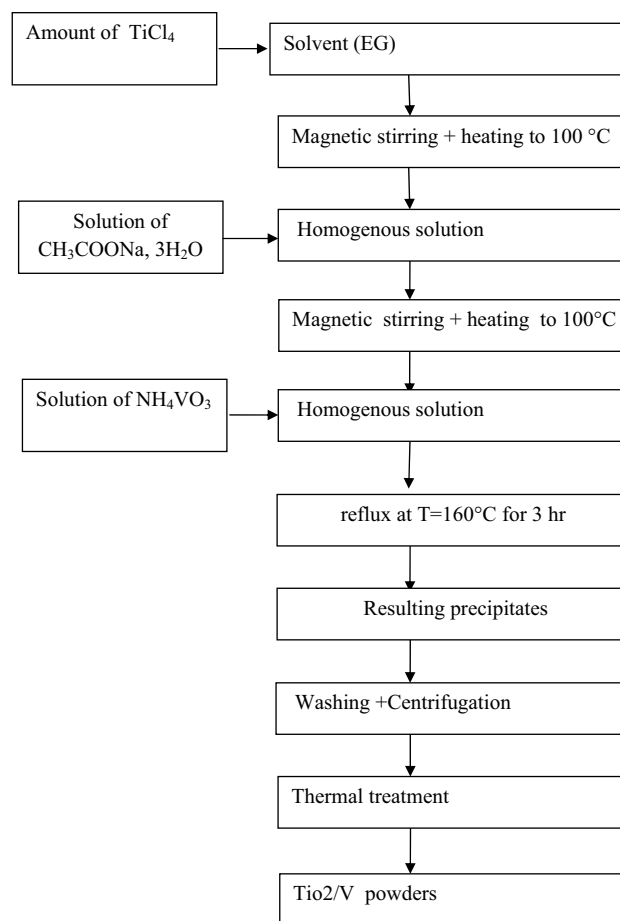


Fig. 1 The flow chart of prepared V-doped TiO_2 by polyol method

to 80° using a step size of 0.02°. The TEM micrographs were obtained on a JEOL 2011 transmission electron microscope with an accelerating voltage of 200 kV. Micro structural characteristics such as morphology Energy-dispersive X-ray analysis (EDX, voltage 20 kV, Takeoff Angle 35.0°) was also used for the chemical analysis of the nanoparticles. Fourier transform infrared (FTIR) spectra were recorded on a Perkin–Elmer Spectrum FTIR spectrophotometer in the range of 400–4000 cm^{-1} . Diffuse reflectance UV–vis absorption spectra (DRS) of powder samples were recorded in the wavelength range 200–800 nm to determine the band gap using UV–vis spectrometer (Shimadzu UV-3101PC) equipped with a diffuse reflectance accessory at room temperature. The thermogravimetric and differential thermal analyses were coupled using TGA Q500 TA instrument. The powder sample (16 mg) was heated starting from 30 °C, reaching 1000 °C using a heating rate of 10 °C min^{-1} under vacuum atmosphere. Excitation and emission spectra of the samples were recorded by photoluminescence spectrophotometer (Avantes, Avaspec-2048-TEC) using a Xenon lamp as excitation source operating at 260 nm.

2.3 Photocatalytic activity measurements

The photocatalytic activities of the V-doped TiO₂ nanoparticles (without catalyst, 2, 4, 6 and 8 mol%) were analyzed based on the photodegradation of MB at room temperature. A medium pressure xenon lamp (150 W) was used as the light source. In a typical photocatalytic experiment, 0.1 g of the sample was dispersed in 100 ml of MB aqueous solution. Before applying the irradiation, the suspension was magnetically stirred for 30 min in the dark to ensure that an adsorption–desorption equilibrium was reached between the V-doped TiO₂ nanoparticles and the aqueous dye solution. Samples of the solution were then collected from the reactor at regular intervals, before centrifuging and analyzing to determine the residual amounts of the dye after photoirradiation using a UV–vis spectrophotometer (Shimadzu UV-2450).

3 Results and discussion

3.1 Structural properties by XRD

The formation of metal oxide nanoparticles synthesized was supported by X-ray diffraction measurements. Figure 2 shows the XRD patterns of TiO₂ samples at different vanadium doped titanium dioxide nanoparticles concentration (2, 4, 6 and 8 mol%). All the observed peaks can be indexed in agreement with the expected tetragonal structure of TiO₂ anatase. The samples are polycrystalline and fit well with the tetragonal crystal structure with space group *I4₁/amd*. The samples show strongest growth along the (101) plane, (004) and (200) planes relatively less dominating to (105), (211), (002), (116) and (220) planes, which matches well with the

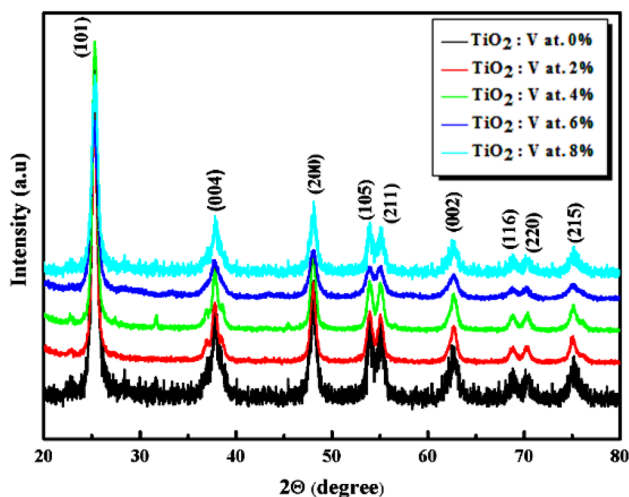


Fig. 2 XRD patterns of titanium oxide (TiO₂) obtained with chemical polyol method using different concentration

data card 77-0447. These results are in good accordance with the findings of Zhifeng et al. [24]. The spectra show that the structure of TiO₂ remains unchanged for low-doping concentration. But, as V doping content increases, the peak position of TiO₂ (101) diffraction shifts to broaden angles, which indicates the decrease of the lattice parameters, this suggests that V ions have substituted, at least partially, in the TiO₂ matrix without changing the tetragonal structure. The lattice constants calculated from the XRD patterns are found to be very close to the TiO₂ ones, i.e. $a=b=3.78 \text{ \AA}$ and $c=9.51 \text{ \AA}$ for the undoped and $a=b=3.78 \text{ \AA}$ and $c=9.48 \text{ \AA}$ to doped powders. The results are summarized in Table 1.

This finding indicates the occurrence of lattice distortion in the anatase structure by the incorporation of the dopants with the smaller ionic radii in TiO₂ matrix, V in oxidation state of +5 has an ionic radius of 0.54 \AA while Ti in +4 oxidation state has an ionic radius of 0.68 \AA [25, 26]. However, the change in the “c” parameter is smaller for doped samples compared to undoped powders, probably because of the different interaction of dopant ions (V) with the Ti ions in the doped powders, moreover The possible interaction between vanadium and titanium are substituted at Ti⁴⁺ sites, location in positions of the lattice interstitial sites rather than directly in Ti⁴⁺ sites and in other case, it seem to be incorporated and dispersed on the surface of TiO₂ crystal matrix. This interaction is relatively depending on ionic radii Vanadium which can easily enter in the site or location. However, in our case those ions seem to be too large to be incorporated in TiO₂ lattice and thus, they are more likely to be found as dispersed metal oxides within the crystal matrix or they are dispersed on the surface of TiO₂.

The lattice constants (a, b and c) of the prepared powders were calculated by employing Eq. (1) [27, 28] given as follows:

$$d_{hkl} = \frac{1}{\sqrt{\frac{h^2+k^2}{a^2} + \frac{1}{c^2}}} \quad (1)$$

where d is the interplanar distance, ‘a’ and ‘c’ are the lattice constants and h, k, l are the Miller indices. It found that the

Table 1 (101) interplanar distance (d_{hkl}), 2θ range and particule dimension (D)

V concentration (mol%)	$d_{(101)}$ (Å)	2θ (degree)	Crystallite sizes (nm)
TiO ₂ pure	3.504	25.41	16.83
TiO ₂ :V at 2%	3.517	25.32	15.1
TiO ₂ :V at 4%	3.521	25.29	14.4
TiO ₂ :V at 6%	3.528	25.24	13.36
TiO ₂ :V at 8%	3.535	25.20	12.27

incorporation of vanadium modifies the transition of anatase to rutile. Choi et al. [29] studied the doping and co-doping of titanium dioxide and reported that it affects the spectra of absorption and photocatalytic activity.

3.2 Transmission electron microscope (TEM)

The TEM micrographs of undoped and V-doped 8 mol% TiO₂ nanoparticles after calcinations at 500 °C for 3 h are shown in Fig. 3a, b. As can be seen from this figure, it can be observed that agglomerates are formed by a superposition of nanometric size particles. For, 8% V-doped TiO₂ powder, the particle size is slightly smaller (12 nm) than that of pure TiO₂ particles (16 nm).

However the EDXS is an excellent tool for the quantitative identification of higher atomic number of elements in the synthesized compound as well as in its grown crystals (Fig. 3c). It confirmed the presence of all non hydrogen elements in the sample: Titanium (Ti), Vanadium (V), Oxygen (O) and small portion of chloride (Cl), sodium (Na) and carbon (C) due to the use of precursors.

3.3 Chemical structure by FTIR

For clarifying whether TiO₂ nanoparticles have corresponding functional groups, the chemical structures of TiO₂ were characterized with FTIR spectroscopy. Figure 4 indicated FTIR spectra of TiO₂ undoped and V-doped. The undoped

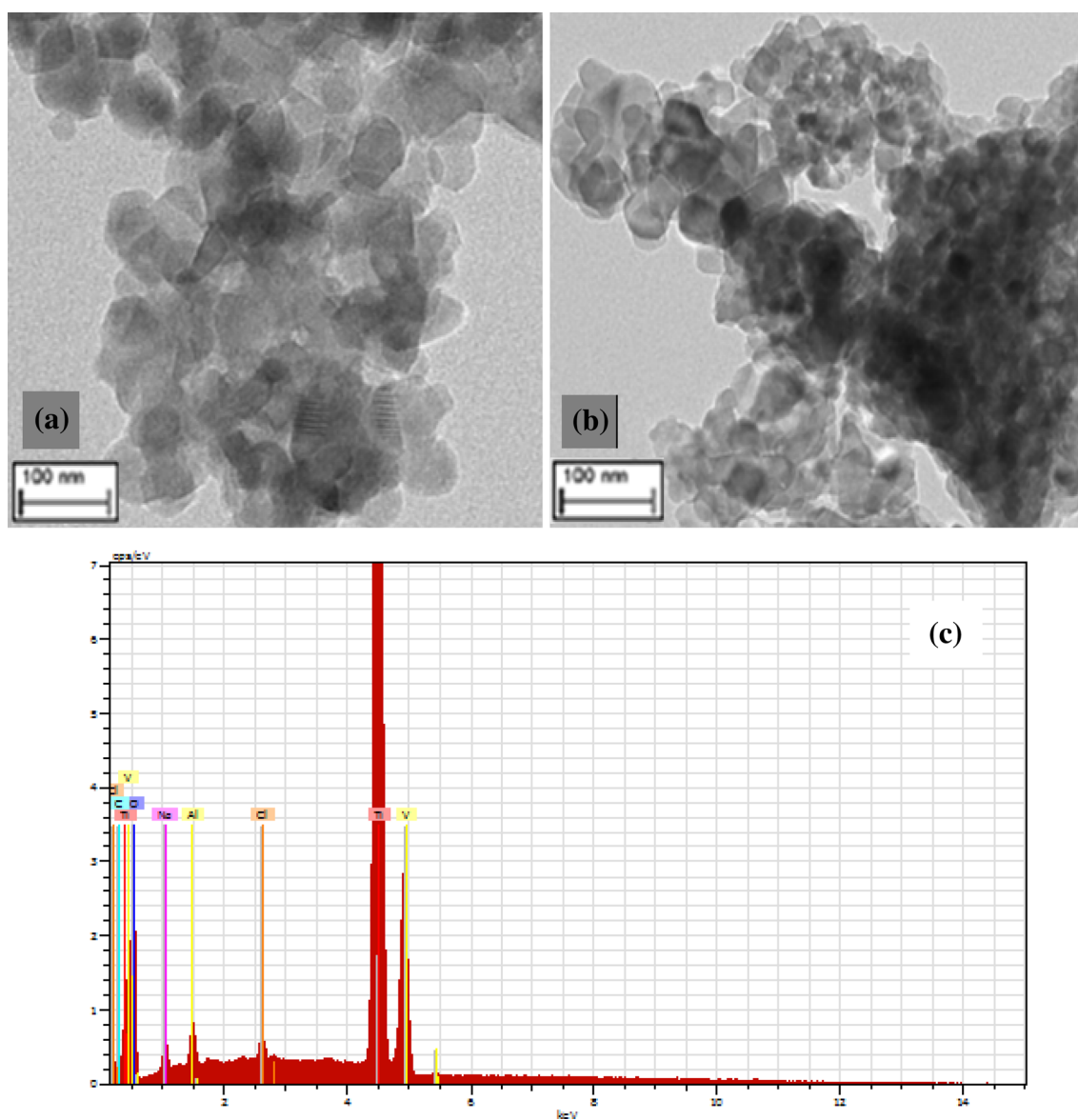


Fig. 3 TEM images (a, b) and a typical EDX spectrum (c) of TiO₂

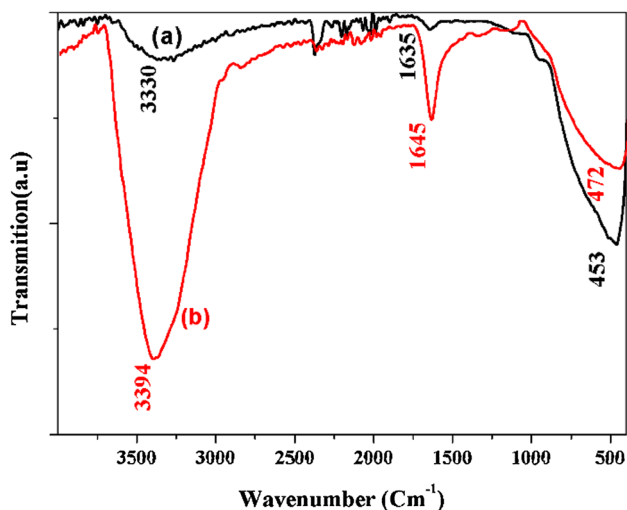


Fig. 4 Spectra FTIR of TiO₂ in both states: undoped (a) and V-doped (b)

sample showed pics at 3300 cm⁻¹ attributed to vibrations (O–H) and pics observed at 1635 cm⁻¹ can be assigned to deformation (O–H) due to water molecules. Notably, the peaks at 453 cm⁻¹ are the contributions from the anatase titania (Fig. 4a). By contrast, upon addition of dopant a small shift was detected for the stretching vibration of Ti–O–Ti was detected after calcinations at 500 °C, According to bibliography the titanium ionic radii is (0.68 Å), on the other hand and V⁵⁺ ion (0.54 Å) [25], smaller than Ti⁴⁺ ion (0.68 Å), would easily incorporates into TiO₂, and enhance a smaller shift in wavenumber of Ti–O–Ti liaison (Fig. 4b).

3.4 Optical properties by UV–vis DRS

UV–vis spectroscopic measurements at room temperature of our samples in the range 200–800 nm were performed (Fig. 5a, b). It indicated that V–TiO₂ absorption spectra extended in the visible region compared to the pure TiO₂. These findings agree well with those obtained by Hoffmann and Choi [29]. Therefore, both the generation of new energy levels due to the injection of impurities within the band gap energies range and the generation of oxygen vacancies by metal doping may contribute to the observed visible light absorption of V–TiO₂ samples.

The absorption coefficient is related to the optical energy band Gap E_g for high photon energies as [30, 31].

$$(\alpha h\nu)^{1/2} = A(h\nu - E_g) \tag{2}$$

where A is a constant and hν is the energy of the incident photon. The plot of (αhν)^{1/2} against (hν) shows a linear dependence. This means that TiO₂ anatase is an indirect transition type semiconductor. The band gap energy (E_g) is

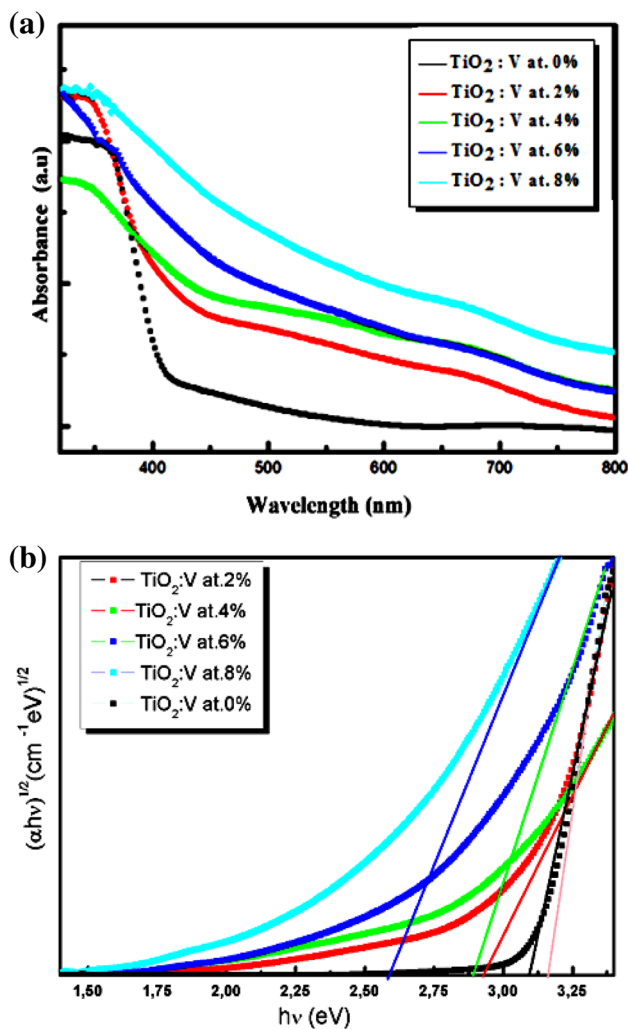


Fig. 5 a UV–vis DRS spectrum and tauc plot (b) of TiO₂ obtained from the chemical polyol method with different concentration

determined by extrapolating the linear part of the spectrum (αhν)^{1/2} curve towards the (hν) axis in Fig. 5b. It is found that the optical band gap of samples shows the decrease of the band gap from 3.18 to 2.6 eV explained by the incorporation of V ions into the TiO₂ lattice. The band-gap energy estimation evidenced the TiO₂ anatase nanostructure (Table 2).

These studies show that doping transition metal ions into TiO₂ could extend the light absorption from UV to the

Table 2 Band gap energy of samples with different vanadium concentrations

Samples	TiO ₂ :V at 0%	TiO ₂ :V at 2%	TiO ₂ :V at 4%	TiO ₂ :V at 6%	TiO ₂ :V at 8%
Energie gap (eV)	3.18	3.09	2.93	2.89	2.60

visible region, leading to the improvement of the photo-response of TiO_2 by introducing additional energy levels within the band gap of TiO_2 . The generation of new energy levels due to the injection of impurities within the band gap energies range resulting in lower band gap.

Therefore, the lower band gap has a positive effect on the photo-catalytic activity because photocatalytic reactions can be activated by photons with lower energy. This can be explicated by the electronic state of dopant and TiO_2 matrix. According to recent proposals suggest and DFT calculations, Electron transition can take place from impurity energy levels ($\text{V}^{5+}/\text{V}^{4+}$) to the conduction band within the band gap of TiO_2 i.e. the impurity level of vanadium lying just below the conduction band of TiO_2 or from the d–d transition of V 3d electrons to Ti 3d [32]. Thus, the new energy levels which are created below the conduction band of TiO_2 are responsible for the activation of the catalyst under visible light illumination.

3.5 Thermal analysis (TGA and DTA)

The findings associated with formation and decomposition phase occurring during heat treatment of synthesized samples of TiO_2 nanoparticles is in good agreement with Thermo Gravimetric Analysis and Differential Thermal Analysis (TGA and DTA) results. Thermal analysis was carried out from room temperature to 1000 °C. TGA of prepared compound was performed by heating the samples in air atmosphere at 10 °C min^{-1} in alumina crucible. Figure 6 displays the thermal analysis (TGA and DTA) for undoped oxide titanium.

As for TiO_2 prepared, there are three distinct mass loss steps in the temperature ranges. The first weight loss step occurred gradually between (50–100 °C). The mass loss was of 7.56%, and this loss of weight is attributed to the removal of water existing on the surface of TiO_2 . Using DTA

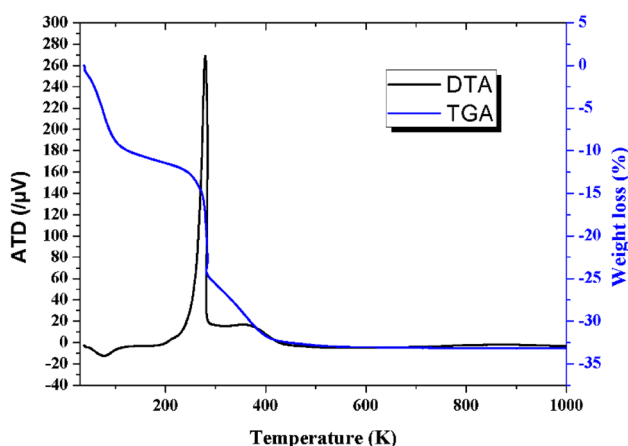


Fig. 6 TGA and DTA curves thermal analysis of amorphous TiO_2

enabled us to find one endothermic peak at 89.82 °C. The second step corresponds to a mass loss (15.04%) occurring at (100–235 °C), which is due to the combustible organic products present in our prepared sample. Through the use of DTA we recorded one endothermic peak at 230.28 °C. The third step stands for a minor weight loss (7.38%) occurring in the range of (250–410 °C), which is due to the transition phase of synthesized compounds. Finally using DTA helped us find one endothermic peak at 406.02 °C. After 410 °C the curve becomes the parallel with the temperature axis which emphasizes high stability of TiO_2 nanoparticles. There is no associated signal with the thermal processes of TiO_2 nanoparticles in the TGA curve confirming the crystallization and phase transition of TiO_2 nanoparticles associated with them.

3.6 Photoluminescence

The PL spectroscopy has been broadly used to study the transition function of the photogenerated carriers in the semiconductors. PL emission spectra have been widely used to investigate the efficiency of charge carrier trapping and migration, and to understand the fact of electron–hole pairs in semiconductors. The measured PL, emission spectra are illustrated in Fig. 7. It exhibits a strong peak at 475 nm, these emission bands originated from charge recombination at the shallow-trap surface state. This surface state originated from the oxygen vacancies which act as radiative centers. The intensity of the PL spectra decreased for 8 wt% V– TiO_2 . This result indicates that the PL-intensity reduction represents the decrease of the photogenerated pairs, recombination process. Broadly speaking, the lower the PL intensity demonstrates the lower recombination rate of the photogenerated electron–hole pairs, which leads to the higher photo-catalytic activity.

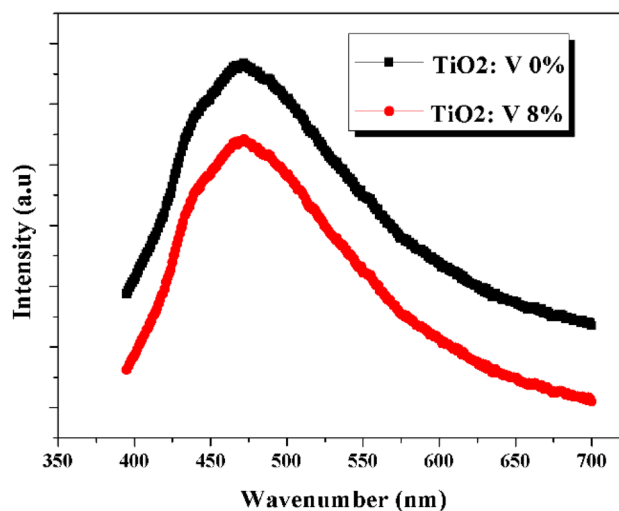


Fig. 7 Emission fluorescence profile of undoped and $\text{TiO}_2\text{:V}$ at 8%

4 Photocatalytic activity

The influence of four different photocatalyst 2% V–TiO₂, at 4% V–TiO₂, at 6% V–TiO₂ and 8% V–TiO₂ on the degradation kinetics of methyl blue was investigated and the results are shown in Fig. 8. It was observed that the blank experiments in under UV-illumination without the nanoparticles were first bearded out to rationalize the photocatalytic activity of the TiO₂ nanoparticles. This, blank experiment result indicated that MB could not be decomposed without the photocatalyst. However the addition of catalysts resulted in obvious degradation of MB.

All the V-doped TiO₂ samples actually exhibited an enhanced photocatalytic activity. In addition, the vanadium content clearly governed the photocatalytic performance of V-doped TiO₂ nanocomposites. The percentage of degradation of MB dye was calculated from the following equation:

$$\text{Percentage of degradation} = (1 - C_t/C_0) \times 100 \quad (3)$$

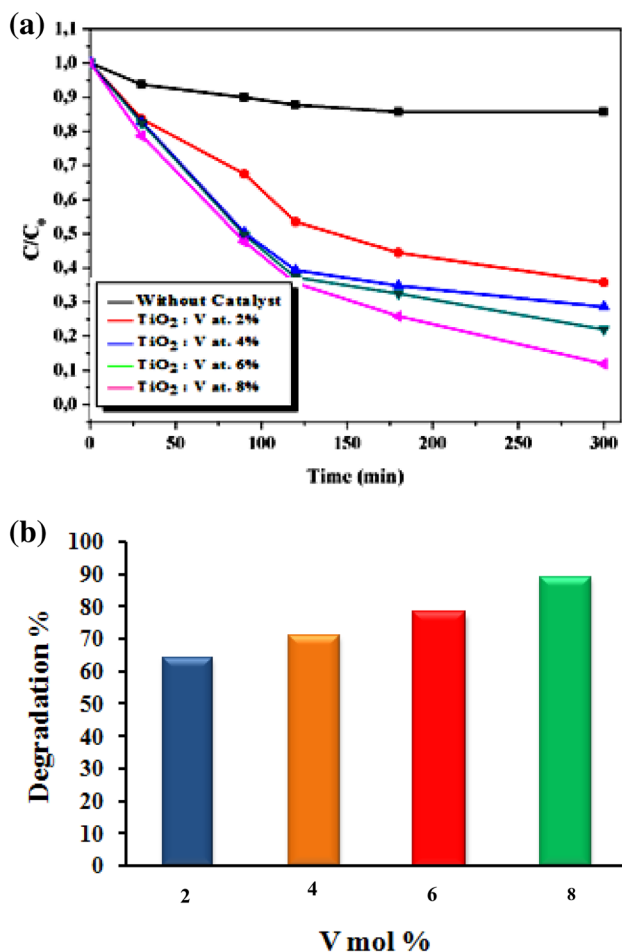


Fig. 8 Photodegradation kinetics (a) and bar diagram for the % degradation (b) of MB dye in the presence of V-doped TiO₂ nanoparticles

where C_0 and C in Fig. 8a represent the initial concentration after the adsorption–desorption equilibrium for 30 min and the real-time concentration of MB, respectively. The photo degradation efficiency of MB was about 64, 71, 78, and 89% at 2% V–TiO₂, at 4% V–TiO₂, at 6% V–TiO₂ and 8% V–TiO₂ respectively (Fig. 8b), when the reaction was performed under UV light for 300 min. In the result, 8% at vanadium content was found to be the optimum concentration.

For a better and more quantitative understanding of the photocatalytic efficiency of the vanadium doped samples, the kinetic analysis [33] of MB degradation was achieved.

Figure 9 implies that the photocatalytic degradation of (MB) obeys the first-order decay kinetics according to the following formula

$$C_0/C = -k \text{ app} \times t.$$

where C_0 is initial concentration of methyl blue (mg/l), C is the concentration of the dye at various interval times (mg/l), t is the illumination time (min) and k is the reaction rate constant. Plotting $\ln(C/C_0)$ versus t gives the apparent constant rate for degradation of methylene blue from the slope of curve fitting line and the intercept is equal to zero. Meanwhile, the linear relationship between $\ln(C/C_0)$ and t indicates that the photocatalytic degradation reaction also follows imply the pseudo first-order reaction.

5 Conclusion

To sum up, we successfully prepared oxide titanium nanoparticles using the straight forward polyol method. The XRD, TEM, FTIR, diffuse reflectance UV–vis spectroscopy, thermal analysis measurements and photoluminescence.

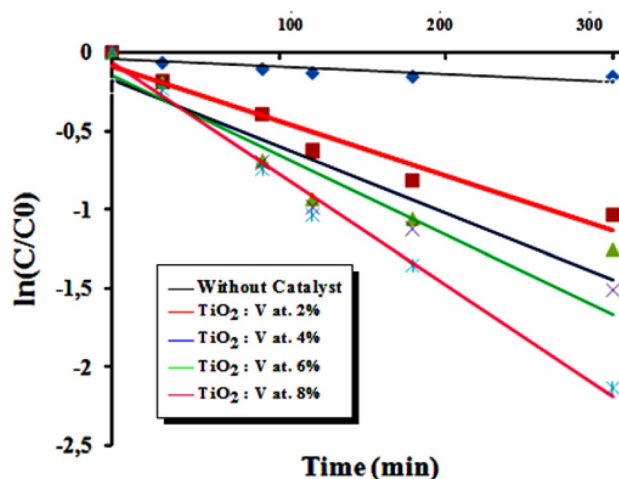


Fig. 9 The pseudo first order kinetics of degradation of methyl blue dye over 2% V–TiO₂, at 4% V–TiO₂, at 6% V–TiO₂ and 8% V–TiO₂ under UV

Vanadium-doped TiO₂ nanopowders showed a tetragonal structure similar to that of undoped TiO₂ with no trace of any other crystalline oxide phase. The average crystallite size of the nanoparticles decreased from 16 to 12 nm when the vanadium content was increased up to 8% suggesting that V-doping subdued the growth of the nanocrystals. Besides, FTIR spectroscopy allowed the observation of oxide titanium band of Ti–O (453 cm⁻¹). Furthermore, 8% V-doped TiO₂ yielded the smallest band gap. In addition TGA results permitted the identification of the thermal cycle of the samples. On the other side, DTA results permitted the identification of the transition temperature phase. The highest photocatalytic activity was obtained with the 8% at V-doped TiO₂.

Acknowledgements Financial support from Unité de Recherche Electrochimie, Matériaux et Environnement UREME (UR17ES45), Faculté des Sciences de Gabès, Université de Gabès, Cité Erriadh, 6072 Gabès, Tunisie.

References

1. S.H. Elder, F.M. Cot, Y. Su, S.M. Heald, A.M. Tyryshkin, M.K. Bowman, Y. Gao, A.G. Joly, M.L. Balmer, A.C. Kolwaite, K.A. Magrini, D.M. Blake, *J. Am. Chem. Soc.* **138**, 1225 (2000)
2. H. Slimen, A. Houas, J.P. Nogier, *J. Photochem. Photobiol. A* **13**, 221 (2011)
3. A. Lassoued, M.S. Lassoued, B. Dkhil, A. Gadri, S. Ammar, *Mol. Struct.* **1148**, 276 (2017)
4. M. Grätzel, *Nature* **414**, 338 (2001)
5. Z. Liu, Y. Li, C. Liu, J. Ya, L.E.W. Zhao, D. Zhao, L. An, *ACS Appl. Mater. Interfaces.* **3**, 1721 (2011)
6. A. Lassoued, M.S. Lassoued, B. Dkhil, A. Gadri, S. Ammar, *Mol. Struct.* **1141**, 99 (2017)
7. S. Sankar, K.G. Gopchandran, *Cryst. Res. Technol.* **44**, 989 (2009)
8. Z. Haddad, C. Abid, H.F. Oztup, A. Mataoui, *Int. J. Therm. Sci.* **76**, 168 (2014)
9. C. Hu, S. Duo, R. Zhang, M. Li, J. Xiang, W. Li, *Mater. Lett.* **64**, 2040 (2010)
10. M.I.B. Bernardi, S. Cava, C.O. Paiva-Santos, E.R. Leite, C.A. Paskocimas, E. Longo, M. Bernardi, *J. Eur. Ceram. Soc.* **22**, 2911 (2002)
11. F. Lan, X. Wang, X. Xu, *React. Kinet. Mech. Catal.* **106**, 113 (2012)
12. F. Morazzoni, C. Canevali, N. Chiodini, C. Mari, R. Ruffo, R. Scotti, L. Armelao, E. Tondello, L. Depero, E. Bontempi, *Mater. Sci. Eng. C* **15**, 167 (2001)
13. A. Lassoued, M.S. Lassoued, B. Dkhil, S. Ammar, A. Gadri, *Physica E* **97**, 328 (2018)
14. M. D'Arienzo, R. Scotti, L. Wahba, C. Battocchio, E. Bemporad, A. Nale, F. Morazzoni, *Appl. Catal.* **93**, 149 (2009)
15. K.S. Kim, S.Y. Yoon, W.J. Lee, K.H. Kim, *Surf. Coat. Technol.* **138**, 229 (2001)
16. J. Zhang, K. Colbow, *J. Appl. Phys.* **71**, 2238 (1992)
17. A. Messad, J. Bruneaux, H. Cachet, M. Froment, *J. Mater. Sci.* **29**, 5095 (1994)
18. H. Kim, A. Pique, *Appl. Phys. Lett.* **84**, 218 (2004)
19. H. Rinnert, P. Miska, M. Vergnat, G. Schmerber, S. Colis, A. Dinia, D. Muller, G. Ferblantier, A. Slaoui, *Appl. Phys. Lett.* **100**, 101908 (2012)
20. R. Bargougui, A. Oueslati, G. Schmerber, C. Ulhaq-Bouillet, S. Colis, F. Hlel, S. Ammar, A. Dinia, *J. Mater. Sci. Mater. Electron.* **25**, 2066 (2014)
21. R. Bargougui, A. Pichavant, J.-F. Hochepped, M.-H. Berger, A. Gadri, S. Ammar, *Opt. Mater.* **58**, 253 (2016)
22. X. Zong, C. Sun, Z. Chen, A. Mukherji, H. Wu, J. Zou, S.C. Smith, G.Q. Lu, L. Wang, *Chem. Commun.* **47**, 6293 (2011)
23. H. Mansour, R. Bargougui, A. Gadri, S. Ammar, *J. Mater. Sci. Mater. Electron.* **2**, 0854 (2016)
24. Z. Liu, Y. Li, C. Liu, J. Ya, E. Lei, W. Zhao, D. Zhao, L. An, *ACS Appl. Mater. Interfaces.* **3**, 1721 (2011)
25. Y. Zhang, G. Li, Y. Wu, Y. Luo, L. Zhang, *J. Phys. Chem. B* **109**, 5478 (2005)
26. J. Arbiol, J. Cerdà, G. Dezaneeau, A. Cirera, F. Peiro, A. Cornet, J.R. Morante, *J. Appl. Phys.* **92**, 853 (2002)
27. H.P. Klug, L.E. Alexander, *X-ray Diffraction Procedures for Polycrystalline and Amorphous Materials* (Wiley, New York, 1974)
28. B.D. Cullity, *Elements of X-ray Diffraction* (Addison Wesley, New York, 1978)
29. W. Choi, A. Termin, M.R. Hoffmann, *J. Phys. Chem.* **98**, 13669 (1994)
30. A. Lassoued, M.S. Lassoued, F. Karolak, S. García-Granda, B. Dkhil, S. Ammar, A. Gadri, *Mater. Sci. Mater. Electron.* **28**, 18480 (2017)
31. J.I. Pankove, *Thin Solid Films.* **90**, 172 (1982)
32. B. Tian, C. Li, F. Gu, H. Jiang, Y. Hu, J. Zhang, *J. Chem. Eng.* **151**, 220 (2009)
33. M.S. Lassoued, A. Lassoued, S.M. Mohammed, S. Abdelbaky, A. Ammar, A. Gadri, S. Ben Salah, S. García-Granda, *Mater. Electron.* **29** 6019 (2018)